Geochemistry, Geophysics, Geosystems

Supporting Information for

Mantle Deformation Processes during the Rift-to-Drift Transition at Magma-Poor Margins

Nicholas J. Montiel[1], Emmanuel Masini[2], Luc Lavier[3], Othmar Müntener[4], and Sylvain Calassou[5]

[1]University of Texas Institute for Geophysics.

[2]M&U France, Grenoble.

[3]University of Texas Institute for Geophysics.

[4]University of Lausanne.

[5]R&D Total Energies.

Contents of this file

Text S1-S6

Figures S1 to S9

Table S1

Additional Supporting Information (Files uploaded separately)

Captions for Movies S1 to S9

Introduction

The supporting information herein consists of figures and tables describing the geometry of each model rifted margin as well as the .vtk files and movies for each model. The figures showing the relationships between surface heat flux, mantle potential temperature, and extension rate to structural and compositional properties of the model rifted margins

were generated using Microsoft Excel. The movies for each model were generated in Paraview using the .vtk files provided here.

Text S1. The mechanical oceanic lithosphere was measured as being from the top of the sedimentary unit to the top of the melt triangle where deformation was localized into a spreading center. Due to the absence of melt extraction in this model, spreading centers were determined to be where anti-listric detachment faults exhumed formerly asthenospheric material (black unit) to the surface.

Text S2. Rift asymmetry was measured as the ratio of the difference between rift flank widths and the overall width of the conjugate margins combined: |left flank – right flank| / (left flank + right flank). The width was defined as the distance between the spreading center and relatively undeformed, minimally attenuated continental crust at the moment of break-up.

Text S3. The scale and frequency sigmoid blocks within anastomosing shear zones was quantified by measuring the width of the smallest block, the largest block, and counting up each block for every model. A single sigmoid block was taken to be a region that was circumscribed by mantle detachment faults within the asthenosphere or sub-continental mantle.

Text S4. Counting crustal allochthons used the same method as described for sigmoid blocks within anastomosing shear zones, but for allochthons defined as blocks of crust or crustal detachments that have been isolated from the continental margin and rest atop mantle material with a detachment fault forming the contact between units.

Text S5. Counting “mantle core complexes” or “mantle megamullions” used the same method as for crustal allochthons and for sigmoid blocks within shear zones. Mantle core complexes or megamullions were defined as regions where the mantle formed a distinct dome that impinged upon or through overlying units along a mantle detachment fault contact.

Text S6. The time between the start of the model and the development of a seafloor spreading center with continentward-dipping, anti-listric faults exhuming formerly asthenospheric material over the shallowest part of the melt triangle was determined to be the time between rift initiation and the drifting phase of ocean basin formation.

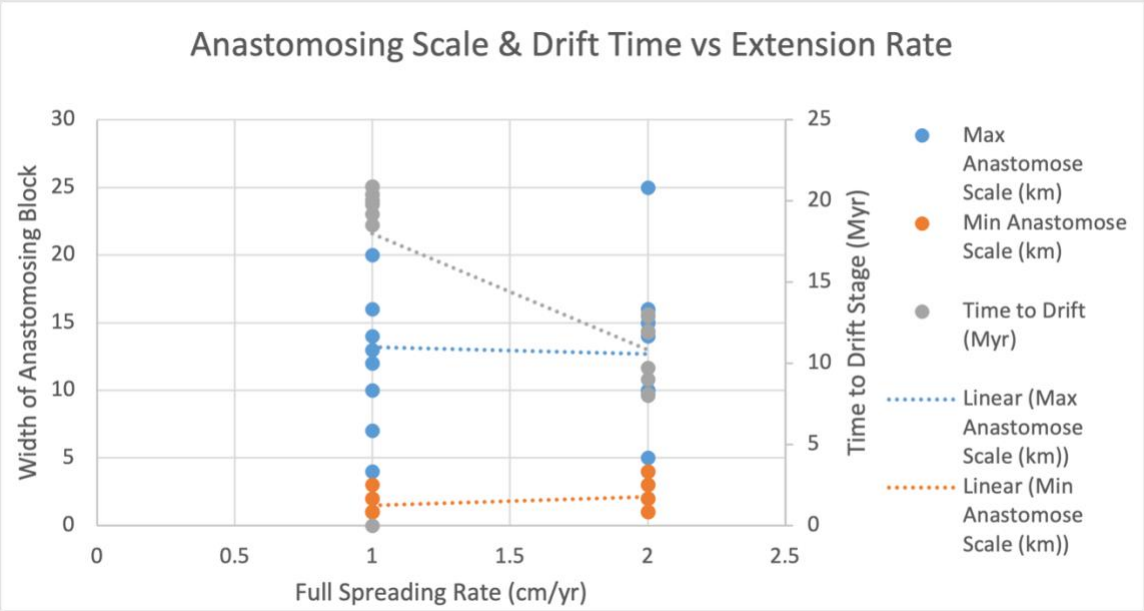

Figure S1. Scatter plot showing the relationships between full-spreading rate, the minimum and maximum scales of sigmoidal, anastamosed blocks, and the time until lithospheric breakup. A linear regression is overlayed on each set. Based on Table S1.

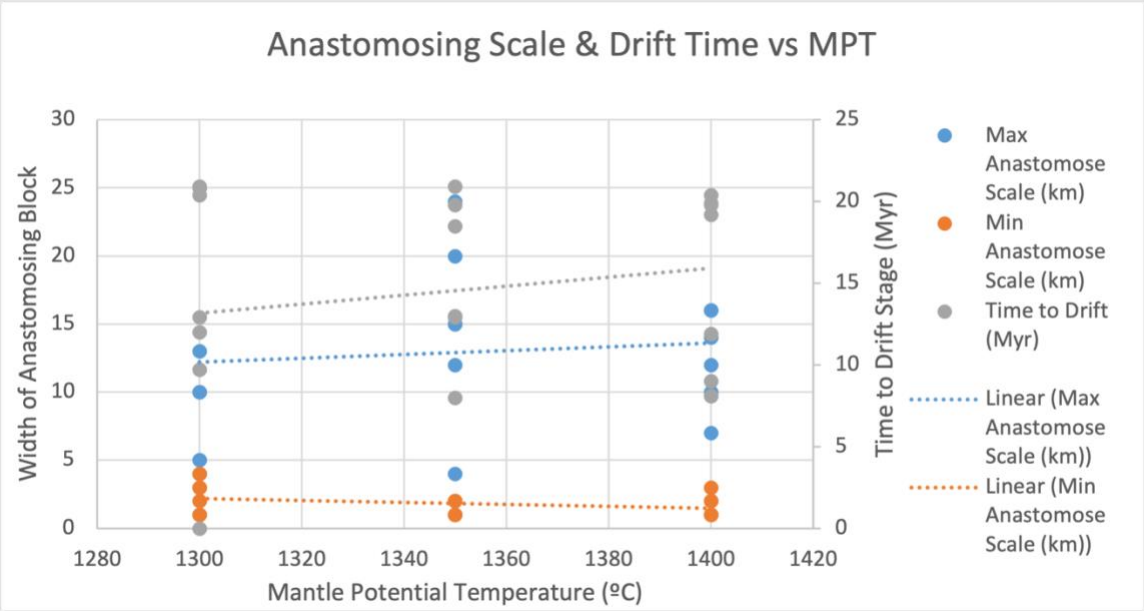

Figure S2. Scatter plot showing the relationships between mantle potential temperature, the minimum and maximum scales of sigmoidal, anastamosed blocks, and the time until lithospheric breakup. A linear regression is overlayed on each set. Based on Table S1.

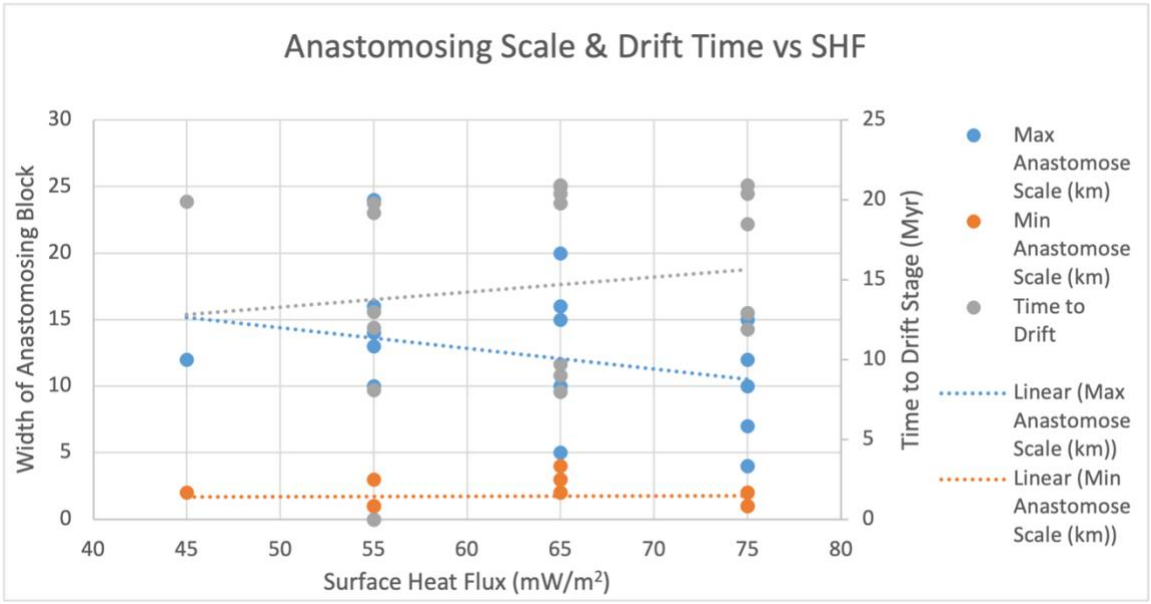

Figure S3. Scatter plot showing the relationships between surface heat flux, the minimum and maximum scales of sigmoidal, anastamosed blocks, and the time until lithospheric breakup. A linear regression is overlayed on each set. Based on Table S1.

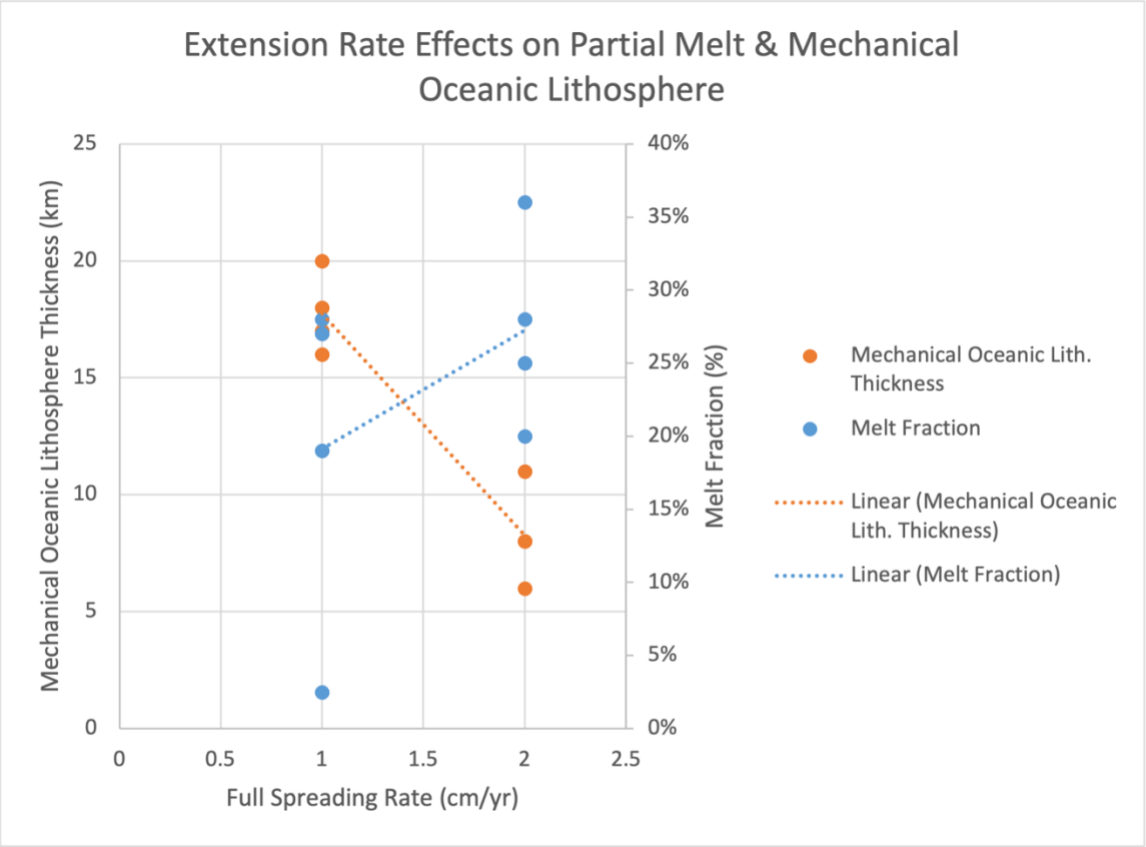

Figure S4. Scatter plot showing the relationships between full-spreading rate, mechanical oceanic lithosphere thickness, and melt fraction as a percentage. A linear regression is overlayed on each set. Based on Table S1.

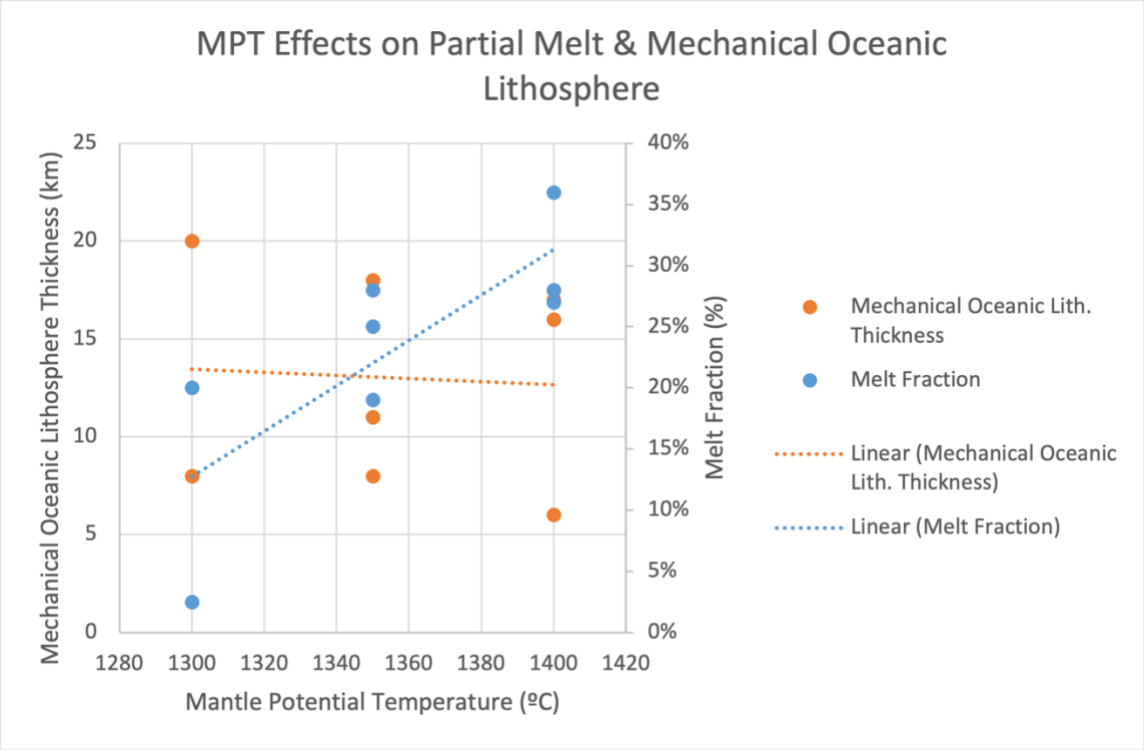

Figure S5. Scatter plot showing the relationships between mantle potential temperature, mechanical oceanic lithosphere thickness, and melt fraction as a percentage. A linear regression is overlayed on each set. Based on Table S1.

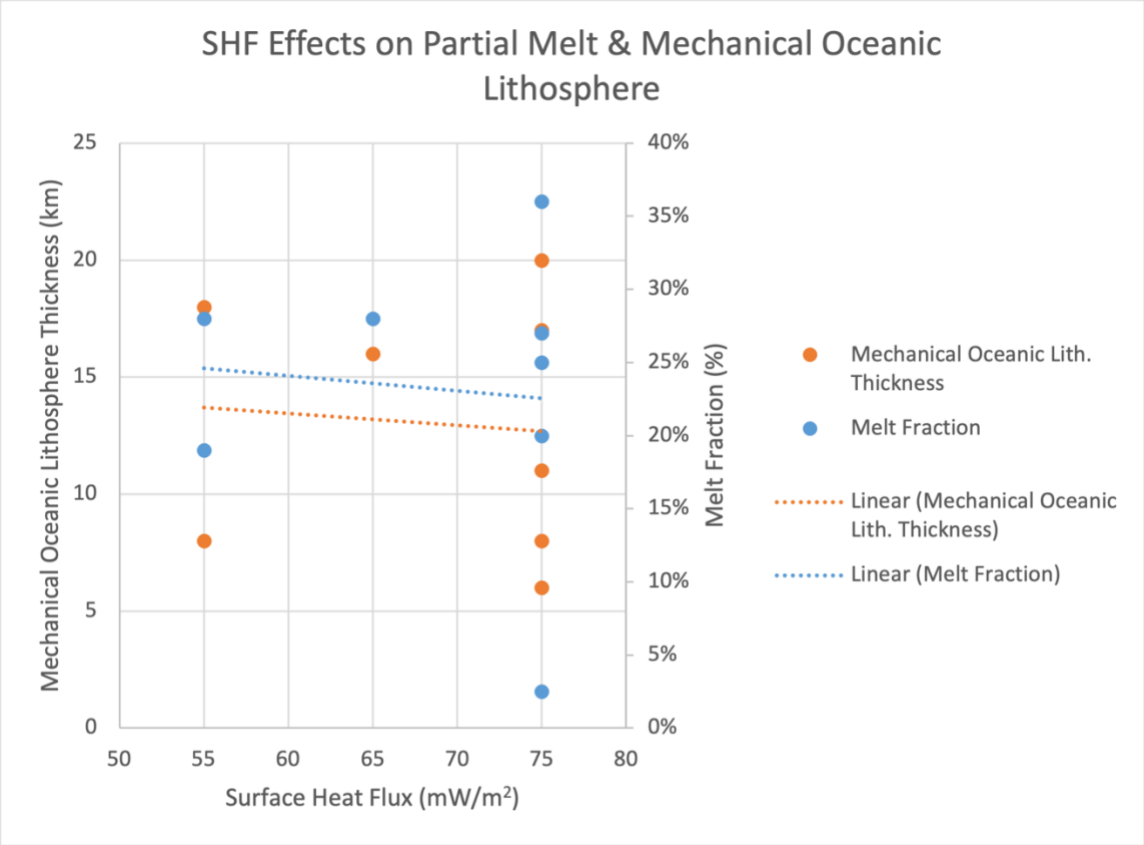

Figure S6. Scatter plot showing the relationships between surface heat flux, mechanical oceanic lithosphere thickness, and melt fraction as a percentage. A linear regression is overlayed on each set. Based on Table S1.

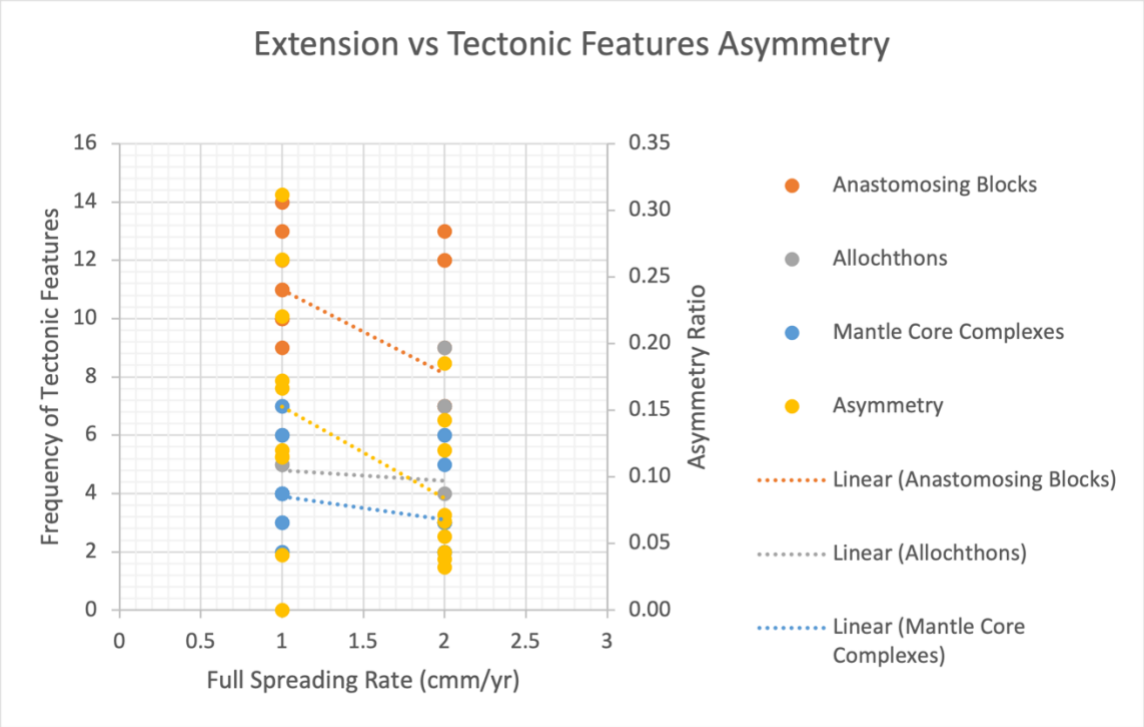

Figure S7. Scatter plot showing the relationships between full-spreading rate, the number of sigmoidal blocks within the anastomosing shear zone, number of crustal allochthons, the number of mantle core complexes, and the degree of asymmetry between the right and left flank widths. A linear regression is overlayed on each set. Based on Table S1.

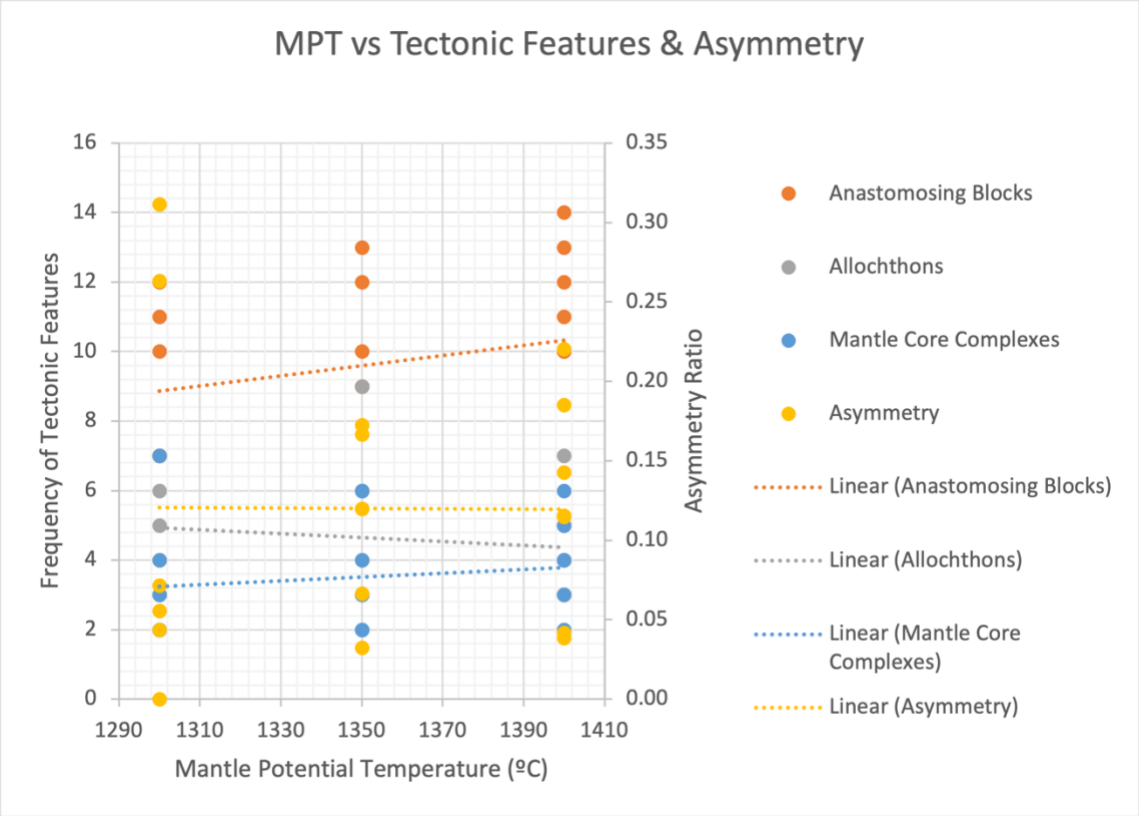

Figure S8. Scatter plot showing the relationships between mantle potential temperature, the number of sigmoidal blocks within the anastomosing shear zone, number of crustal allochthons, the number of mantle core complexes, and the degree of asymmetry between the right and left flank widths. A linear regression is overlayed on each set. Based on Table S1.

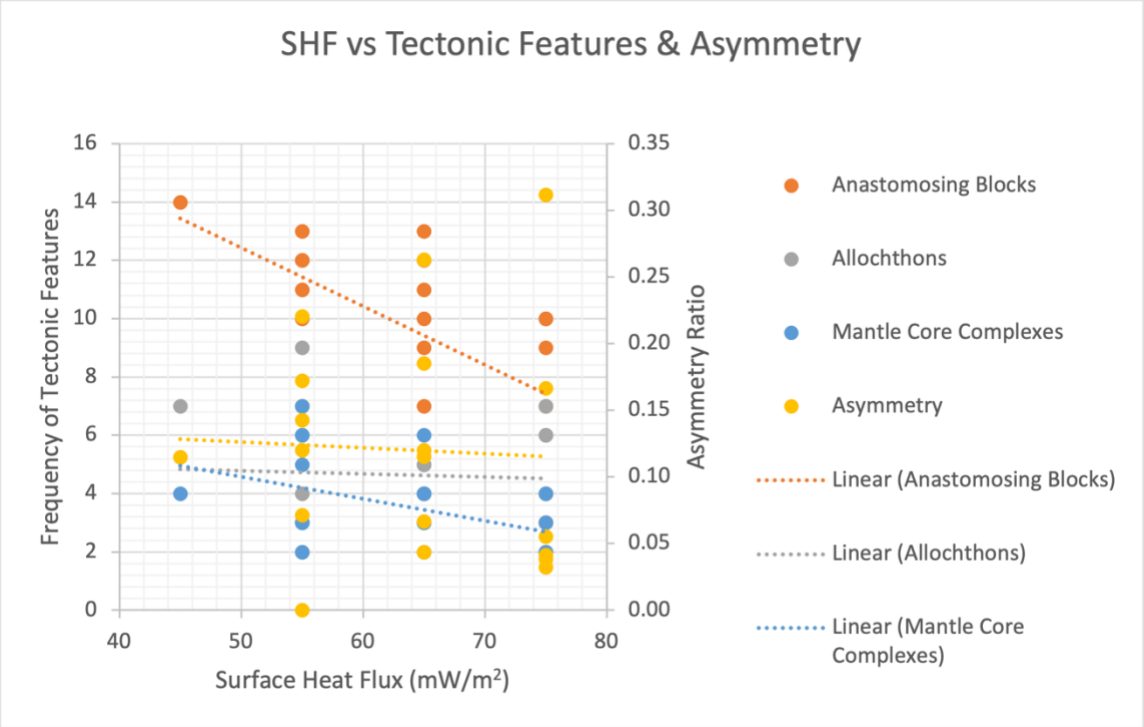

Figure S9. Scatter plot showing the relationships between surface heat flux, the number of sigmoidal blocks within the anastomosing shear zone, number of crustal allochthons, the number of mantle core complexes, and the degree of asymmetry between the right and left flank widths. A linear regression is overlayed on each set. Based on Table S1.

Model	MPT (ºC)	SHF (mW/m^2	Extension Rate (cm/yr)	% Partial Melt	Ocean Lith. Thick. (km)	Left Flank Width (km)	Right Flank Width (km)	Asymmetry	Anastomosing/Duplex Blocks	Crustal Boudins/Allochthons	Max Anastomose Scale (km)	Min Anastomose Scale (km)	Mantle Core Complexes/Megamullions	Time to Drift (Myr)
1	1300	55	2	19%	10	150	130	0.07	7	3	25	3	2	12
2	1300	65	1	8.3%	16	105	180	0.26	12	5	10	3	4	20.4
3	1300	65	2	20.0%	9	120	110	0.04	7	3	5	4	2	9.7
4	1350	65	1	20.0%	19	110	140	0.12	10	4	20	2	4	20.9
5	1350	65	2	31%	6	120	105	0.07	9	3	15	1	3	8
6	1350	75	1	22%	12	100	140	0.17	9	6	12	2	2	18.5
7	1400	45	1	32%	15	170	135	0.11	14	7	16	1	4	19.9
8	1400	55	1	35%	14	115	180	0.22	10	4	14	1	3	19.2
9	1400	55	2	35%	10	120	90	0.14	12	2	16	2	5	8.1
10	1400	65	2	32%	11	160	110	0.19	13	4	10	3	6	9
11	1300	55	1	0%	NaN	NaN	NaN	NaN	11	6	13	1	7	NaN
12	1350	55	1	19%	18	170	120	0.17	13	3	24	1	6	19.8
13	1350	55	2	28%	8	140	110	0.12	12	9	15	2	3	13
14	1400	65	1	28%	16	115	145	0.12	11	5	12	1	3	19.8
15	1300	75	1	3%	20	105	200	0.31	10	4	4	1	2	20.9
16	1400	75	1	27%	17	125	115	0.04	10	4	7	2	4	20.4
17	1300	75	2	20%	8	190	170	0.06	7	7	10	2	3	12.9
18	1350	75	2	25%	11	150	160	0.03	3	6	4	1	2	12.9
19	1400	75	2	36%	6	125	135	0.04	3	3	14	1	2	11.9

Table S1. Table containing all of the measured quantities for Models 1-19 and used as the basis for Figs. S1-S9. The NaN values for Model 11 are due to seafloor spreading center never developing and deformation never localizing in a single rift axis for this case.

Data Set S1. The animation of the phase evolution of Model 1.

Data Set S2. The animation of the phase evolution of Model 2.

Data Set S3. The animation of the phase evolution of Model 3.

Data Set S4. The animation of the phase evolution of Model 4.

Data Set S5. The animation of the phase evolution of Model 5.

Data Set S6. The animation of the phase evolution of Model 6.

Data Set S7. The animation of the phase evolution of Model 7.

Data Set S8. The animation of the phase evolution of Model 8.

Data Set S9. The animation of the phase evolution of Model 9.

Data Set S10. The animation of the phase evolution of Model 10.

Data Set S11. The animation of the phase evolution of Model 11.

Data Set S12. The animation of the phase evolution of Model 12.

Data Set S13. The animation of the phase evolution of Model 13.

Data Set S14. The animation of the phase evolution of Model 14.

Data Set S15. The animation of the phase evolution of Model 15.

Data Set S16. The animation of the phase evolution of Model 16.

Data Set S17. The animation of the phase evolution of Model 17.

Data Set S18. The animation of the phase evolution of Model 18.

Data Set S19. The animation of the phase evolution of Model 19.